

pubs.acs.org/acscatalysis Research Article

Influence of Brønsted Acid-Site Density on Reaction-Diffusion Phenomena that Govern Propene Oligomerization Rate and Selectivity in MFI Zeolites

Elizabeth E. Bickel, Songhyun Lee, and Rajamani Gounder*



Cite This: ACS Catal. 2023, 13, 1257-1269



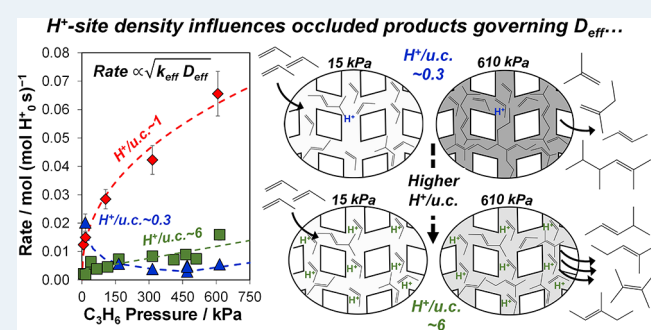
ACCESS I

III Metrics & More

Article Recommendations

Supporting Information

ABSTRACT: Brønsted acid zeolites catalyze propene oligomerization to higher-molecular-weight alkenes. Previous studies that only consider kinetic factors have reached contradictory conclusions regarding the dependence of oligomerization rates on H⁺-site density in MFI zeolites. Herein, we account for both the reaction and diffusion phenomena that govern the rates and selectivity of propene oligomerization and interrogate suites of MFI samples synthesized with widely varying H⁺-site density (0.3–5.7 H⁺/unit cell; Si/Al 13–250) and crystallite size (0.03–2.65 μ m). Heavier alkene products become occluded within zeolitic micropores during reaction and impose intrazeolite diffusional restrictions for all MFI samples over wide ranges of reaction conditions (483–523 K, 7–615 kPa C₃H₆). This occluded organic



...and thereby oligomerization rates, reaction orders, and selectivity

phase becomes heavier in composition at higher propene pressures and lower reaction temperatures, which favor the growth of higher-molecular-weight oligomers, resulting in effective diffusivities of propene and product alkenes that systematically decrease with increasing propene pressure. Analysis of product selectivity reveals that MFI samples of lower H⁺-site density possess higher rate constant ratios for trimerization relative to dimerization, leading to the formation of heavier alkenes within their micropores and, in turn, to a greater decrease in the effective diffusivity of propene and product alkenes with increasing propene pressure. As a result, measured dimerization rates on MFI samples, which convolve the influences of kinetic factors and intrazeolite diffusional constraints imposed by the occluded organic phase, exhibit an increasingly negative-order dependence on propene pressure with decreasing H⁺-site density. The combined influences of kinetic factors and intrazeolite diffusional constraints result in different dependences of oligomerization rate on H⁺-site density when measured at different propene pressures, reconciling apparent contradictions among previous reports. Overall, these findings reveal the strong influences of H⁺-site density in MFI zeolites on both the kinetics of propene oligomerization reactions and the composition of the product-derived intrazeolite organic phase that influences effective diffusivities, and consequently measured propene oligomerization rates and product selectivity.

KEYWORDS: deactivation, zeolites, heterogeneous catalysts, oligomerization, diffusion

1. INTRODUCTION

Brønsted acid zeolites catalyze propene oligomerization, an important reaction for upgrading light alkenes into fuel-range hydrocarbons.¹ Propene oligomerization rates and selectivity have been reported to depend on various zeolite properties, including the density^{2–5} and distribution^{3,6} of H⁺ sites and the zeolite topology,⁷ but mechanistic proposals are discordant among these reports. Mlinar et al. reported that propene conversion (25 kPa C₃H₆, 513 K) measured at a fixed space velocity (4 mol C₃ (mol Al s)⁻¹) systematically decreased with increasing Al content on commercially sourced H-MFI samples (Si/Al 13–140) and attributed this to lower rates of trimerization caused by steric crowding from nearby adsorbates, which expectedly increase in density with H⁺-site content.² Bernauer et al. crystallized suites of MFI samples with varied Al content (Si/Al 13–30) and different fractions of

proximal H⁺ sites (\geq 0.45 or \leq 0.25, assessed by Co²⁺ titration, 3 × 24 h, 0.05 M Co(NO₃)₂, ambient temperature) using mixtures of tetrapropylammonium (TPA⁺) and Na⁺ structure-directing agents and various Si and Al sources,³ and reported propene consumption rates (per Al, 22 kPa C₃H₆, 533 K) that decreased systematically with Al content for MFI samples that contained similar fractions of proximal Al. Propene consumption rates (per Al) also decreased with the fraction of

Received: October 20, 2022 Revised: December 13, 2022 Published: January 5, 2023





proximal Al for MFI samples of lower Al content (Si/Al ~30) but were invariant with the fraction of proximal Al for MFI samples of higher Al content (Si/Al ~13).³ Conversely, Sarazen et al. reported propene consumption rates (per H⁺, 75 kPa C_3H_6 , 503 K) that were independent of Al content on commercially sourced MFI samples (Si/Al 14–140), concluding that propene dimerization rates were kinetically limited under these conditions,⁷ but that product selectivities could be influenced by intrazeolite diffusional constraints.⁴ Corma et al. reported that, among commercially sourced MFI samples, smaller crystallites and higher Al contents led to higher propene conversions and attenuated catalyst deactivation during propene oligomerization at high conversions (X = 40-90%, 473 K, 4000 kPa C_3H_6).⁵

The different dependences of propene oligomerization rates on H+-site (or Al) density reported among previous studies are contradictory if rates are interpreted to be kinetically limited, as done in these studies.^{2,3,7} In contrast, our recent work showed that propene dimerization rates and selectivity measured over a wide range of reaction conditions (15-615 kPa C₃H₆, 503 K) on MFI and other 10-membered-ring (10-MR) zeolites (TON, MEL) were influenced by intrazeolite diffusion limitations, even at nominally differential reaction conditions and at the earliest stages of reaction, as evident in rates (per H⁺) that decreased systematically with increasing crystallite size $(0.1-2.7 \mu m)$ for MFI samples crystallized with fixed H⁺-site density in the limit of dilute H⁺ sites (H⁺/unit cell (u.c.) ~ 0.3 , Si/Al ~ 250). Measured propene dimerization rates (per H⁺) on MFI samples of fixed H⁺-site density (H⁺/ u.c. ~0.3) increased linearly with inverse crystallite length, which is the functional dependence expected from the effectiveness factor expression in the limit of strong intrazeolite mass transfer limitations.8 Importantly, the complete regeneration of H-MFI catalysts in inert flow at reaction temperature (503 K), in conjunction with transient changes in dimerization rates observed upon step-changes in reaction temperature or propene pressure, revealed that intrazeolite diffusion limitations resulted from the accumulation of heavier oligomerization products within zeolitic micropores, which decreased the effective diffusivities of propene and product alkenes during oligomerization.⁸ The influence of intrazeolite diffusional constraints imposed by the occluded product-derived organic phase during propene oligomerization is also consistent with observations of product diffusional constraints during 1-butene oligomerization on H-Beta (498 K)⁹ and 1-hexene oligomerization on H-MFI (\leq 473 K).¹⁰

Herein, we study propene oligomerization over a wide range of reaction conditions (7-615 kPa C₃H₆, 483-523 K) on suites of MFI samples crystallized with fixed H+-site density $(H^+/u.c. = 0.3, 1.3, or 5.7)$ and varied crystallite sizes (0.03-2.65 μ m) to interrogate the effects of H⁺-site density on propene dimerization rates and selectivity. Dimerization rates on MFI samples of a wide range of H⁺-site densities (0.3-5.7 H+/u.c.) are found to be governed by intrazeolite diffusion limitations imposed by alkene products occluded within zeolitic micropores that decrease the effective diffusivity of propene and product alkenes, consistent with our prior results on MFI samples of dilute H⁺-site content (H⁺/u.c. ~ 0.3). Effectiveness factor formalisms together with product selectivity analysis are used to explore the dependence of effective diffusivities on propene pressure and H+-site density and the influence of H⁺-site density on the composition of the occluded organic phase that regulates intrazeolite diffusion.

Kinetic measurements reveal different dependencies of dimerization rates on propene pressure among MFI samples of varied H+-site density. Importantly, accounting for the coupled influences of kinetic factors and diffusional constraints imposed by occluded alkene products enables rationalizing the different dependences of dimerization rate on propene pressure among MFI samples of varied H⁺-site density, and reconciling the seemingly contrasting dependences of propene oligomerization rates on H+-site density in MFI reported among previous studies. Together, these findings demonstrate the preeminent role of the intrazeolite organic phase formed during propene oligomerization catalysis in governing the effective diffusivity of propene and product alkenes, and thereby measured oligomerization rates and selectivity, as well as the dependence of the composition of this phase on H⁺-site density in MFI zeolites.

2. EXPERIMENTAL SECTION

2.1. Synthesis of H-MFI Samples. Samples are denoted MFI-X-Y ($X = \text{approximate } H^+/\text{unit cell (u.c.)}, Y = \text{mean}$ crystallite size in μ m). The synthesis methods used to crystallize MFI-0.3-Y samples were reported previously.8 An MFI sample containing higher Al content (Si/Al 13, MFI-5.7-0.30) was obtained from a commercial source (Zeolyst, CBV2314). MFI-1.3-Y samples were synthesized by adapting previously reported methods. 11 To synthesize MFI-1.3-0.33, a synthesis gel was prepared with molar ratios of 1 SiO₂/0.009 Al₂(SO₄)₃/0.078 NaOH/0.18 TPAOH/29 H₂O. To prepare this synthesis gel, 14.5 g of tetrapropylammonium hydroxide solution (TPAOH, Alfa Aesar 40 wt/wt % in H₂O), 4.91 g of sodium hydroxide solution (NaOH, Sigma-Aldrich, 97 wt %, 10 wt/wt % in deionized H_2O (18.2 $M\Omega$)), and 58.8 g of deionized H2O were combined and stirred until homogenized in a perfluoroalkoxy alkane (PFA) jar. In a separate PFA jar, 0.952 g of aluminum sulfate octadecahydrate (Al₂(SO₄)₃· 18H₂O, Sigma-Aidrich, \geq 97%) was dissolved in 10 g of deionized H₂O and added dropwise to the first solution. Finally, 32.7 g of tetraethyl orthosilicate (TEOS, Aldrich, 98%) was added to the mixture and stirred for 24 h under ambient conditions. The synthesis solution was then transferred to a 45 cm³ Teflon-lined stainless-steel autoclave (Parr Instruments) and placed in a forced convection oven at 443 K for 24 h under rotation (60 rpm).

To synthesize MFI-1.3-0.06, a synthesis gel was prepared with molar ratios of 1 $SiO_2/0.010$ $Al_2(SO_4)_3/0.092$ NaOH/ 0.25 TPAOH/13 H₂O. To prepare the synthesis gel, 31.8 g of tetrapropylammonium hydroxide solution (TPAOH, Alfa Aesar 40 wt/wt % in H_2O), 0.92 g of sodium hydroxide (NaOH, Sigma-Aldrich, 97 wt %), and 26.4 g of deionized H₂O were combined and stirred until homogenized in a PFA jar. In a separate PFA jar, 1.67 g of aluminum sulfate octadecahydrate ($Al_2(SO_4)_3 \cdot 18H_2O$, Sigma-Aidrich, $\geq 97\%$) was dissolved in 10 g of deionized H₂O and added dropwise to the first solution. Finally, 52.1 g of tetraethyl orthosilicate (TEOS, Aldrich, 98%) was added to the mixture and stirred for 24 h under 353 K. The synthesis solution was then transferred to a 45 cm³ Teflon-lined stainless-steel autoclave and placed in a forced convection oven at 433 K for 24 h under rotation (60 rpm).

MFI-1.3-0.03 was synthesized using a gemini-type quaternary ammonium surfactant (C_{666} , C_6H_{13} – N^+ (CH_3)₂– C_6H_{12} – N^+ (CH_3)₂– C_6H_{13} ·2Br⁻), which was prepared following previously reported methods. ¹² A synthesis gel was prepared

with molar ratios of $1 \, \mathrm{SiO_2/0.010} \, \mathrm{Al_2(SO_4)_3/0.18} \, \mathrm{NaOH/0.10} \, \mathrm{C_{666}/40} \, \mathrm{H_2O}$. To prepare the synthesis gel, $1.68 \, \mathrm{g}$ of $\mathrm{C_{666}}$, $2.40 \, \mathrm{g}$ of sodium hydroxide solution (10 wt/wt % NaOH, Sigma-Aldrich, 97 wt % in deionized $\mathrm{H_2O}$), and $13.7 \, \mathrm{g}$ of deionized $\mathrm{H_2O}$ were combined and stirred until homogenized in a PFA jar. In a separate PFA jar, $0.22 \, \mathrm{g}$ of aluminum sulfate octadecahydrate ($\mathrm{Al_2(SO_4)_3\cdot18H_2O}$, Sigma-Aidrich, $\geq 97\%$) was dissolved in 5 g of deionized $\mathrm{H_2O}$. The aluminum sulfate solution was added dropwise to the first solution. Finally, $5.01 \, \mathrm{g}$ of colloidal silica (Ludox AS40, 40 wt/wt %, Sigma-Aldrich) was added to the mixture and stirred for $12 \, \mathrm{h}$ under ambient conditions. The synthesis solution was then transferred to a 45 cm³ Teflon-lined stainless-steel autoclave and placed in a forced convection oven at 403 K for 7 days under rotation (60 rpm).

Synthesized solids were recovered via centrifugation and washed with deionized water until the pH of the supernatant reached a value below 8. Samples were treated in flowing air at 853 K (0.0167 K s⁻¹) for 10 h (6.9 \times 10⁻⁵ mol s⁻¹, UHP, 99.999%, Indiana Oxygen) to remove occluded organic content.

2.2. Characterization of H-MFI Samples. The topology of crystallized MFI samples was assessed by powder X-ray diffraction (XRD). XRD patterns were collected using low dead-volume sample holders (Rigaku) and a scan rate of 0.04° s⁻¹ on a Rigaku SmartLab X-ray diffractometer with a Cu K α radiation source ($\lambda = 0.154$ nm) operating at 1.76 kW. The crystallinity of MFI samples was assessed by calculating micropore volumes from N₂ adsorption isotherms (77 K) measured with a Micromeritics 3Flex Adsorption Analyzer. Samples were degassed by heating under vacuum to 393 K, holding isothermally for 2 h, heating under vacuum to 623 K, and again holding isothermally for 9 h. Micropore volumes were estimated by extrapolating the uptake of liquid N_2 (P/P_0 = 0.05-0.90, 77 K) on degassed samples to zero pressure and from a semilogarithmic derivative plot of the isotherm given by $\partial(V_{ads})/\partial(\ln(P/P_0))$ in which the volume of adsorbed N₂ at the first minimum corresponds to the pressure at which micropores have been filled. Micropore volumes estimated by both methods agreed within $\pm 5\%$.

An FEI Quanta 3D FEG Dual-beam SEM instrument equipped with an Everhart–Thornley detector for high vacuum imaging (2–7 kV) and a spot size range of 1–5 μ m was used to collect scanning electron microscopy (SEM) images. Mean crystallite size was taken to be the average length of the shortest dimension of the crystallite measured for \geq 30 crystallites.

Temperature-programmed desorption (TPD) of NH₃ using NH₄-form samples was used to quantify the number of H⁺ sites. NH₄-form samples were prepared by aqueous ion exchange in a 1 M NH₄NO₃ solution (100 cm³ g_{sample}⁻¹, NH₄NO₃ \geq 98%, Sigma-Aldrich, 24 h). Exchanged samples were washed with deionized water (30 cm³ g_{sample}⁻¹, 4×) and dried overnight at 373 K in stagnant air. In TPD experiments, NH₄-form samples were held at 323 K for 0.5 h under flowing He (\sim 1 × 10⁻⁵ mol s⁻¹, 99.999%, Indiana Oxygen). The temperature was increased to 873 K (at 0.167 K s⁻¹) while quantifying the NH₃ desorbed.

 Co^{2+} titrations were performed by aqueous ion exchange with 0.5 M $\text{Co}(\text{NO}_3)_2$ solution (150 cm³ g_{sample}^{-1} , 99%, Sigma-Aldrich, 353 K, 24 h) according to previously reported methods.¹³ Co-exchanged samples were washed with deionized water (30 cm³ g_{sample}^{-1} , 5×), and dried overnight at 373 K

in stagnant air. Inductively coupled plasma optical emission spectroscopy (ICP-OES) was used to quantify Al and Co using a Thermo Fisher Scientific iCAP 7000 Series ICP-OES spectrometer. Samples were prepared by digesting 0.01–0.02 g of sample in 2.0–3.0 g of hydrofluoric acid solution (48 wt %) for 24 h and subsequently adding 45–55 g of deionized water and approximately 1 g of nitric acid (40 wt %). [Caution: appropriate personal protective equipment, ventilation, and other safety measures should be used when working with HF]. Elemental compositions were determined using standards of known concentration to generate calibration curves.

2.3. Propene Reactions on H-MFI Samples. Propene reactions were performed in a stainless-steel reactor (9.5 mm i.d.) held within a furnace with a concentric thermowell containing a K-type thermocouple extending through the axial center with the tip of the thermocouple located in the center of the catalyst bed. Pressure upstream of the catalyst bed was controlled with a back-pressure regulator located downstream. Reactant flows were composed of 5-95% propene (99.99%, Matheson), 5% methane (99.97%, Matheson) as an internal standard, and balance argon (99.999%, Indiana Oxygen). Reactor effluent flowed through resistively heated lines (410 K) to a gas chromatograph equipped with a flame ionization detector (Agilent 7890A, GS GasPro column, 0.320 mm i.d., X 60 m \times 0 μ m). Products were quantified with methane as an internal standard with injections beginning after 7-12 min time-on-stream.

To prepare the catalyst bed, NH₄-form zeolite was pelletized and sieved to retain particles of fixed diameter (180–250 μ m) (0.01-0.06 g). These particles were mixed with SiO₂ (180-250 μm, Sigma-Aldrich, high-purity grade) in zeolite/SiO₂ weight ratios of 0.03-0.15. This mixture was loaded into the stainless-steel reactor, supported between quartz wool plugs and stainless-steel rods on both sides. Prior to oligomerization, an oxidative pretreatment $(1.7 \times 10^{-5} \text{ mol s}^{-1} \text{ flowing air (air }$ zero, THC < 1 ppm) and flowing 5.1×10^{-5} mol s⁻¹ Ar (99.999%, Indiana Oxygen)) was performed to convert the sample into its H-form by ramping the temperature to 823 K (0.025 K s⁻¹) and subsequently cooling to reaction temperature (483–523 K). Space velocity was varied at fixed propene partial pressure by changing the mass of catalyst loaded (0.01– 0.06 g) and the flow rate of propene $(8 \times 10^{-6} \text{ to } 5 \times 10^{-5} \text{ mol})$ s⁻¹). Fresh catalyst was loaded and used to measure the rate at each reaction condition unless otherwise noted. Dimerization rates were estimated from rates of product formation using eq 1 where r_n is the rate of formation of products of carbon number n to account for the formation of products other than

$$r_{\text{dim}} = r_6 + r_9 + r_{12} + \frac{1}{2}(r_4 + r_5 + r_7 + r_8 + r_{10} + r_{11})$$
(1)

Detailed discussion of eq 1 is available elsewhere. Absolute uncertainties in rate measurements were estimated by propagating the uncertainties associated with catalyst loading, the initial number of H^+ sites (H_0^+) quantified with NH $_3$ TPD, and the uncertainty in relative GC peak areas estimated from the fluctuation of the reactant peak area relative to the internal standard peak area in GC analysis of the reactant stream while bypassing the reactor. Rates are reported at their steady-state values unless otherwise noted. Dimerization rates reached steady-state values after ~ 80 to 100 ks for most samples (Section S6, SI), but continued to change slightly with time for

some samples. For such samples, the steady-state rate was taken to be the rate value after dimerization rates changed <4% over 8 ks.

3. RESULTS AND DISCUSSION

3.1. Presence and Origin of Intrazeolite Diffusional Constraints on MFI Samples of Varying H⁺-Site Density and Crystallite Size. The physicochemical properties of the MFI samples studied herein are summarized in Table 1;

Table 1. Physicochemical Properties of MFI Zeolite Samples Used in This Study

sample ^a	Si/Al ^b	H ⁺ /u.c. ^c	$\mathrm{length}^d/\mu\mathrm{m}$	std. dev. $^e/\mu$ m
MFI-5.7-0.30 ^f	13	5.7	0.30	0.11
MFI-1.3-0.03	47	1.3	0.03	0.01
MFI-1.3-0.06	54	1.4	0.06	0.01
MFI-1.3-0.33	55	1.4	0.33	0.05
MFI-0.3-0.13	290	0.3	0.13	0.02
MFI-0.3-0.31	343	0.3	0.31	0.04
MFI-0.3-0.89	298	0.4	0.89	0.13
MFI-0.3-2.65	222	0.4	2.65	0.32

^aSample nomenclature is MFI-X-Y, $X = H^+/u.c.$, $Y = average length of the shortest crystallite dimension in <math>\mu$ m. ^bDetermined by ICP-OES. ^cEstimated by NH₃ TPD. ^dAverage length and ^estandard deviation of the shortest crystallite dimension estimated by SEM; particle size distributions in Figure S4, SI. ^fCommercial sample, Zeolyst CBV2314.

samples are denoted MFI-X-Y (X = approximate H⁺/unit cell (u.c.), Y = mean crystallite size in μ m). MFI samples of varied crystallite size (0.03–0.33 μ m) and fixed Al content (Si/Al ~50) were synthesized by adapting previously reported synthetic methods. X-ray diffraction (XRD) patterns and micropore volumes measured from N₂ adsorption isotherms for MFI-1.3-Y samples were consistent with the MFI topology (Sections S1 and S2, SI). The number of H⁺ sites was quantified by NH₃ temperature-programmed desorption and was similar to the Al content (\geq 0.85, Table S1) for all but one sample (further discussion in Section S4, SI), indicating most Al on these samples was located in framework positions.

Crystallite size distributions were determined for these samples (Figure S4a-c) from SEM images; the mean crystallite size (L) was taken to be the average length of the shortest dimension measured for \geq 30 crystallites. The synthesis methods used to crystallize MFI-0.3-Y samples, as well as characterization and crystallite size distributions for these samples, are reported elsewhere. An MFI sample containing higher Al content (Si/Al 13, MFI-5.7-0.30) was obtained from a commercial source (Zeolyst, CBV2314), with characterization data reported elsewhere. Together, these samples comprise a suite of MFI materials with varied crystallite sizes (0.03–2.65 μ m) at different H⁺-site densities (0.3, 1.3, or 5.7 H⁺/u.c.).

Propene dimerization rates were estimated from rates of product formation for MFI-1.3-Y samples (eq 1). Dimerization rates decreased with time (Figure 1a) for all samples and over the course of many turnovers (Figure S7, SI), and then approached a steady-state rate (taken to be the value after rates changed less than 4% over 8 ks), indicating some form of apparent catalyst deactivation with time. Initial dimerization rates were measured by extrapolating dimerization rates to zero time-on-stream following the procedures outlined in previous reports. 8,9,14,15 Dimerization rates (per H₀, 503 K) compared either at initial or steady-state conditions decreased systematically with increasing crystallite size (Figures 1a,b and S9, SI), indicating that measured rates are limited by intrazeolite diffusion since other catalyst properties that might influence dimerization rates (e.g., H+-site density) are fixed among these samples. These findings are consistent with dimerization rates (per H⁺) that systematically decreased with crystallite size for MFI samples of more dilute Al content (Si/Al ~250, H⁺/u.c. \sim 0.3) under similar conditions (503 K, 15–615 kPa C₃H₆) as we previously reported.8

The influence of intrazeolite diffusion on measured dimerization rates on MFI-1.3-Y samples was further substantiated using the effectiveness factor formalism. An effectiveness factor expression was derived assuming dimerization is intrinsically first-order in propene pressure and

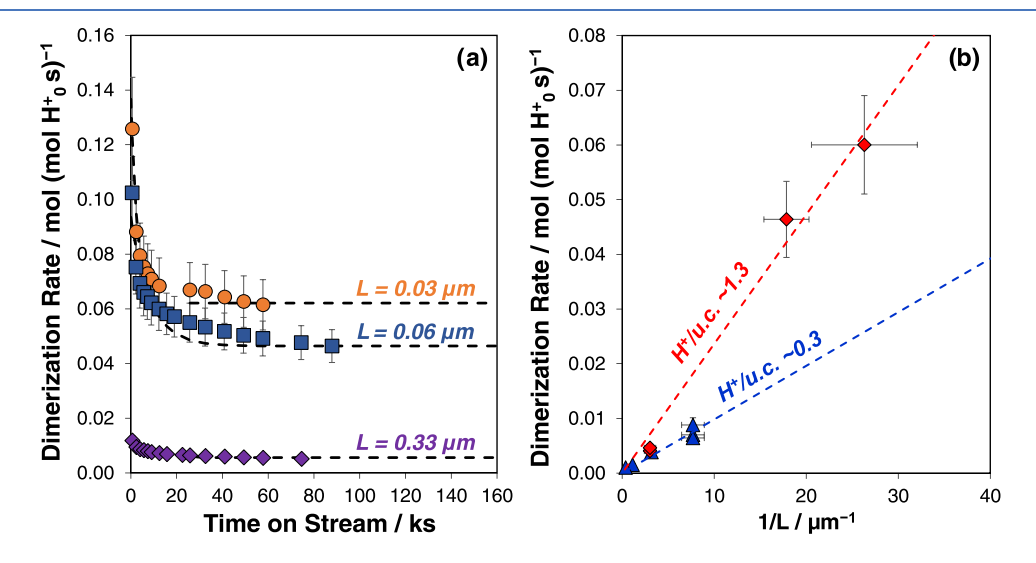


Figure 1. Dimerization rates measured at 503 K, 315 kPa C_3H_6 (a) plotted against time on stream for MFI-1.3-0.03 (circles), MFI-1.3-0.06 (squares), MFI-1.3-0.33 (diamonds), (b) steady-state dimerization rates plotted against inverse crystallite size for MFI-1.3-Y samples (diamonds) and MFI-0.3-Y samples (triangles) (rates measured on MFI-0.3-Y samples originally reported in Bickel and Gounder⁸). Dashed lines represent linear regressions to eq 2.

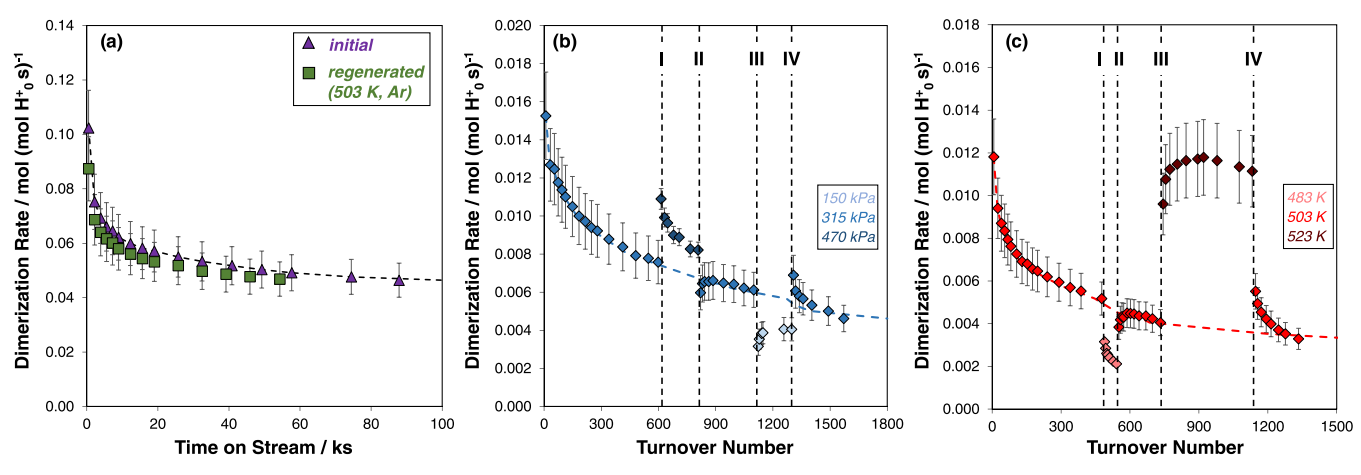


Figure 2. (a) Dimerization rates measured (503 K) on MFI-1.3-0.06 (triangles) upon initial exposure to propene, and after regeneration in flowing Ar (47 ks, squares) at 503 K. (b) Dimerization rates measured (503 K) on MFI-1.3-0.33. Black dashed lines represent step-changes in the pressure. (I) 315 \rightarrow 470 kPa, (II) 470 \rightarrow 315 kPa, (III) 315 \rightarrow 150 kPa, (IV) 150 \rightarrow 315 kPa. Blue dashed lines represent an interpolation of rates at 315 kPa. (c) Dimerization rates measured (315 kPa C_3H_6) on MFI-1.3-0.33. Black dashed lines represent step-changes in the temperature. (I) 503 \rightarrow 483 K, (II) 483 \rightarrow 503 K, (III) 503 \rightarrow 523 K, (IV) 523 \rightarrow 503 K. Red dashed lines represent an interpolation of rates at 503 K. Error bars reflect absolute error.

crystallites are of slab geometry, for the limit of strong diffusion limitations ⁸

$$r_{\text{dim, meas}} = \sqrt{\frac{k_{\text{eff}} D_{\text{e}}}{[H_0^+]}} C_{3s} \frac{2}{L}$$
 (2)

In eq 2, k_{eff} is the effective dimerization rate constant, which is a function of the intrinsic dimerization rate constant and equilibrium constants for adsorption (eqs S5-S7, SI), C_{3s} is the fluid-phase concentration of propene, $[H_0^+]$ is the initial H⁺-site density (per crystallite volume), D_e is the effective diffusivity of propene, and L is the crystallite size. Steady-state (Figure 1b, diamonds) and initial (Figure S9, SI) dimerization rates measured on MFI-1.3-Y samples increased linearly with inverse crystallite size, as predicted by eq 2. Moreover, the slope of the linear regression to eq 2 was lower for steady-state rates than for initial rates (Figure S9, SI), consistent with intrazeolite diffusion limitations that become more severe with increasing time-on-stream.8 Intrazeolite diffusion limitations were not expected for MFI-1.3-Y samples per the Weisz-Prater criterion estimated assuming the effective diffusivity of propene is equal to the single-component effective diffusivity of propane¹⁷ in otherwise vacant MFI micropores (10⁻⁵–10⁻³ ≪ 1, Section S9, SI), suggesting these intrazeolite mass transfer limitations result from the pernicious influence of occluded heavier hydrocarbons on the effective diffusivity of propene and product alkenes, as we have reported previously for MFI samples of dilute H⁺-site density (H⁺/u.c. \sim 0.3).

Regeneration experiments were performed to determine the nature of species responsible for the decrease in dimerization rates with time on MFI-1.3-Y samples during propene oligomerization. A representative MFI-1.3-Y sample (MFI-1.3-0.06) was exposed to propene oligomerization reaction conditions (503 K, 315 kPa C_3H_6) for 87 ks and subsequently exposed to flowing inert gas at reaction temperature (503 K, 47 ks, 7×10^{-5} mol Ar s⁻¹). Treatment with inert gas at reaction temperature led to the full recovery of dimerization rates (within ca. 1.05×, Figure 2a) and their transient decrease with time-on-stream. An inert purge at reaction temperature was also able to regenerate an MFI sample of higher Al content (MFI-5.7-0.30, Figure S8, SI). The ability of an inert purge at

reaction temperature to regenerate the catalyst is consistent with previous observations for MFI samples of dilute H⁺-site density (\sim 0.3) and indicates that the decrease in measured dimerization rates with time among MFI samples of widely varying compositions (H⁺/u.c. 0.3–5.7, Si/Al \sim 13 to 250) occurs through the reversible accumulation of alkene products during alkene oligomerization, rather than deactivation by products with high degrees of unsaturation (e.g., polyaromatics). 8,18,19

To understand the mechanism through which accumulated alkene products influence measured dimerization rates, dimerization rates were measured with intervening stepchanges in propene pressure or reaction temperature. Dimerization rates were first measured on a representative MFI-1.3-Y sample (MFI-1.3-0.33) at 315 kPa for ~65 ks, after which propene pressure was increased to 470 kPa for ~20 ks (Figure 2b(I)) and then decreased back to 315 kPa (Figure 2b(II)). Propene pressure was then decreased to 150 kPa for ~45 ks (Figure 2b(III)) and increased back to 315 kPa (Figure 2b(IV)). A similar experiment was also performed for an MFI sample of higher H⁺-site density (MFI-5.7-C) (Section S10, SI). Dimerization rates were also measured on MFI-1.3-0.33 at fixed propene pressure (315 kPa, 503 K) with intervening stepchanges in temperature (Figure 2c). The temperature was first decreased to 483 K (Figure 2c(I)) and held for ~20 ks before increasing again to 503 K (Figure 2c(II)). The temperature was subsequently increased to 523 K (Figure 2c(III)) and held for 35 ks before decreasing again to 503 K (Figure 2c(IV)). Step-decreases in propene pressure (Figure 2b(II)) and stepincreases in reaction temperature (Figure 2c(II)) led to dimerization rates that were initially lower than their expected values (blue and red dashed lines in Figure 2b,c, respectively), and increased over the course of many turnovers to achieve those values. Conversely, step-increases in propene pressure (Figure 2b(IV)) and step-decreases in temperature (Figure 2c(IV)) led to rates that were initially higher than their expected values and decreased over the course of many turnovers to achieve those values. Transient changes in rates persisted for a larger number of turnovers upon a step-decrease in propene pressure or a step-increase in temperature, compared to upon a step-increase in propene pressure or a

step-decrease in reaction temperature (e.g., Figure 2b(II) vs (IV), Table S2, SI).

Higher propene pressures and lower reaction temperatures preferentially increase rates of oligomerization reactions relative to rates of β -scission reactions, thereby resulting in heavier compositions of alkene products formed and accumulated within the MFI micropores. 4,8,15,20-22 The lower rates measured immediately upon a step-decrease in propene pressure or a step-increase in reaction temperature indicate that the heavier alkene products decrease the effective diffusivities of propene and product alkenes.8 These heavier products persist within zeolitic micropores following a stepdecrease in propene pressure or a step-increase in reaction temperature until they slowly diffuse out of the zeolitic micropores (or undergo β -scission to smaller fragments that diffuse). Eventually, a lighter composition of occluded products characteristic of the new reaction conditions is established, resulting in a gradual increase in dimerization rates with time (Figure 2b(II),c(II)). These findings are consistent with the similar transient changes in rates upon step-changes in propene pressure or temperature observed for MFI samples of more dilute Al content (Si/Al \sim 250, \sim 0.3 H⁺/u.c.). Together, the full regeneration of MFI samples by an inert purge at reaction temperature and the transient rate changes observed upon step-changes in reaction conditions evince that the decrease in propene dimerization rates with time in MFI samples of varying compositions (Si/Al ~13 to 250) reflects the accumulation of heavier alkene products, which impose intrazeolite diffusion limitations by decreasing the effective diffusivity of propene and product alkenes relative to their single-component effective diffusivities. Transient changes in dimerization rate upon step-changes in reaction conditions indicate that the heavier composition of occluded products formed at higher propene pressures and lower reaction temperatures results in more severe intrazeolite diffusion limitations.

3.2. Variation in Intrazeolite Diffusional Constraints among H-MFI Samples of Varied H⁺-Site Density. The dependence of dimerization rates on crystallite size was evaluated for H-MFI samples of different Al content to determine how H⁺-site density influences the reactivity of H⁺ sites for propene oligomerization and intrazeolite diffusion. Steady-state dimerization rates measured on samples of high and low H⁺-site density (H⁺/u.c. \sim 1.3 vs 0.3) increased linearly with inverse crystallite size (Figure 1b); yet the slope of a linear regression to eq 2 differed between these samples (by ca. 3×). This slope depends on the initial H⁺-site density ([H₀⁺], eq 2), which is a known quantity and can be eliminated by multiplying the measured dimerization rate by the square root of the H⁺-site density to obtain a parameter κ

$$\kappa = r_{\text{dim,meas}} \sqrt{[H_0^+]} = \sqrt{k_{\text{eff}} D_{\text{e}}} C_{3s} \frac{2}{L}$$
(3)

The value of κ measured under fixed reaction conditions (503 K, 315 kPa C_3H_6) is plotted against inverse crystallite size in Figure 3 for samples of fixed H⁺-site density (H⁺/u.c. ~0.3, 1.3) and varied crystallite size. An MFI sample of higher H⁺-site density (MFI-5.7-0.30) was also included in Figure 3 since pressure step-change experiments indicated rates were strongly limited by intrazeolite mass transfer on this sample (further discussion in Section S10, SI). The slope of linear regressions to eq 3 increased systematically with increasing H⁺-site density (Figure 3), indicating differences in the effective dimerization

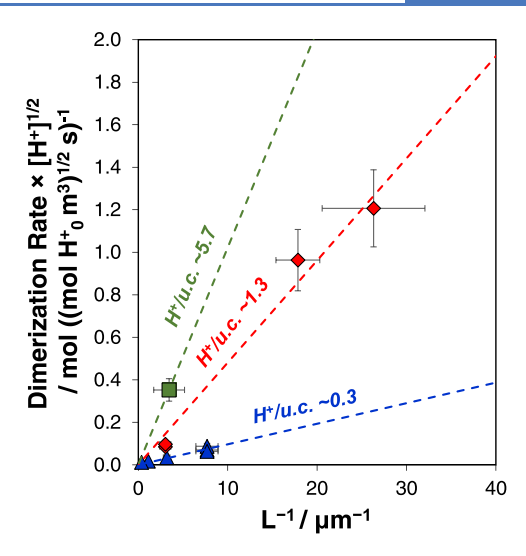


Figure 3. Values of κ calculated from steady-state dimerization rates measured at 503 K, 315 kPa C_3H_6 on suites of MFI samples of fixed H⁺-site density and varied crystallite size: MFI-0.3-Y samples (triangles), MFI-1.3-Y (diamonds), MFI-5.7-0.30 (squares). Dashed lines indicate fits of data measured on samples of fixed H⁺-site density to eq 3.

rate constant ($k_{\rm eff}$) or effective diffusivity of propene ($D_{\rm e}$) among MFI samples of different H⁺-site density (eq 3).

To further elucidate the influence of H⁺-site density on dimerization rates, a parameter, ξ , was calculated from the slopes of the linear regressions to eq 3, which depends only on the effective dimerization rate constant $(k_{\rm eff})$ and the effective diffusivity of propene $(D_{\rm e})$.

$$\xi = \sqrt{k_{\text{eff}} D_{\text{e}}} \tag{4}$$

Steady-state dimerization rates were measured on MFI samples of fixed H⁺-site density and varied crystallite size (Figures S10–S11, SI) at different propene pressures, to determine the dependence of ξ (eq 4) on propene pressure and H⁺-site density (Figure 4a). The value of ξ systematically decreased with increasing propene pressure for MFI samples of all H⁺-site densities. Since the effective dimerization rate constant ($k_{\rm eff}$) is not expected to change with propene pressure, ⁸ this change in ξ indicates that the effective diffusivity of propene decreases with increasing propene pressure. Notably, this conclusion is independently corroborated by the results of the pressure stepchange experiments (Section 3.1), which imply that effective diffusivities of propene decrease with increasing propene pressure because such reaction conditions lead to the formation of heavier occluded products.

Values of ξ at a given propene pressure varied with H⁺-site density, indicating that the effective dimerization rate constant ($k_{\rm eff}$), the effective diffusivity of propene ($D_{\rm e}$), or both are influenced by H⁺-site density (eq 4). Higher H⁺-site densities have been documented to increase the self-diffusivity of propene in microporous voids (SAPO-34, 295 K) because of favorable interactions between the π -bond of propene and H⁺ sites; ²³ however, H⁺ sites are covered with propene-derived surface intermediates under the reaction conditions studied herein (483–523 K, 7–615 kPa C_3H_6), ⁷ precluding such effects. Importantly, different relationships between ξ and H⁺-site density were observed at high and low propene pressures (e.g., ~16 and 315 kPa, Figure 4b,c, respectively). At low propene pressures (\leq 16 kPa C_3H_6), values of ξ were the

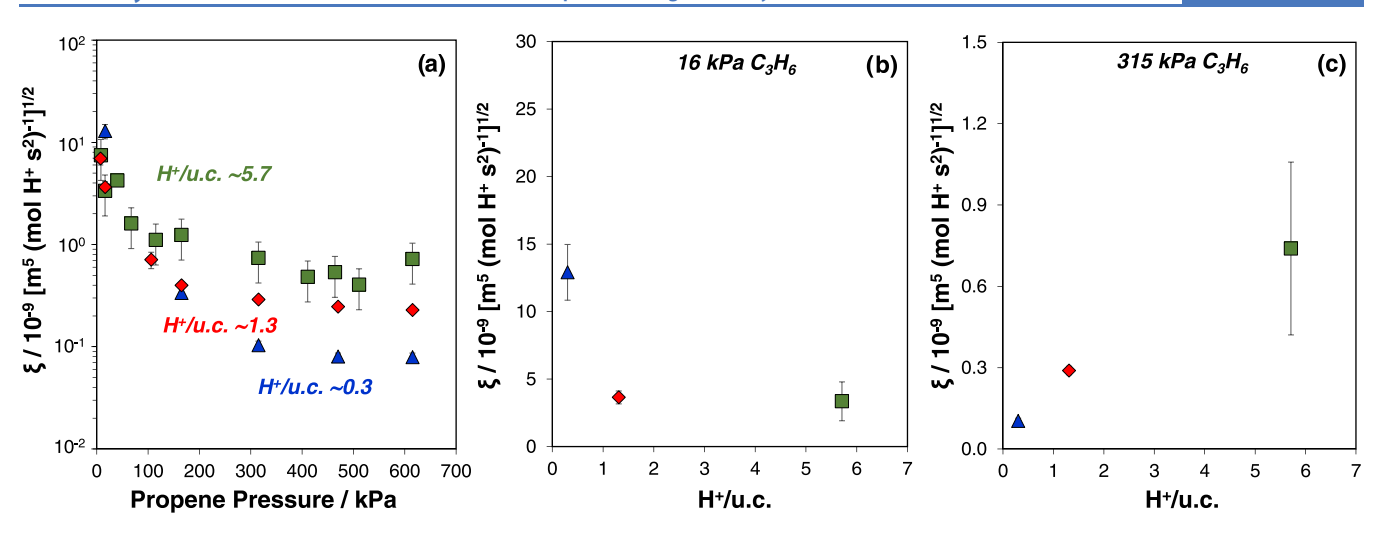


Figure 4. (a) Values of ξ (503 K) estimated from steady-state dimerization rates for MFI samples of different Al content: MFI-0.3-Y samples (triangles), MFI-1.3-Y (diamonds), and MFI-5.7-0.30 (squares) plotted against propene pressure. (b) Values of ξ (503 K, 16 kPa C_3H_6) for MFI samples of different $H^+/u.c.$ (c) Values of ξ (503 K, 315 kPa C_3H_6) for MFI samples of different $H^+/u.c.$ Error bars reflect absolute error.

highest for MFI samples of the lowest H+-site density (MFI-0.3-Y samples, Figure 4b). In contrast, at higher propene pressures (≥ 165 kPa C_3H_6), values of ξ increased systematically with H⁺-site density (e.g., 315 kPa C₃H₆, Figure 4c). Changes in ξ among MFI samples of different H⁺-site densities (Figure 4) cannot be rationalized by a difference in only the effective dimerization rate constant or only the effective diffusivity of propene because a difference in only one of these parameters should have resulted in the same dependence of ξ on H⁺/u.c. at all propene pressures. Thus, changes in ξ with H⁺-site density must reflect convoluted influences of H⁺-site density on the kinetic properties of H⁺ sites and on the composition of the occluded organic phase governing the effective diffusivity of propene and product alkenes. To assess the possible influences of H+-site density on the effective dimerization rate constant and effective diffusivity, we next analyze differences in product composition among MFI samples of varied H+-site density.

3.3. Product Composition on MFI Samples of Fixed Crystallite Size and Varied H⁺-Site Density. The propene oligomerization reaction network is shown in Scheme 1, beginning with propene dimerization to form the primary reaction product (C_6) . Dimers can undergo higher-rank reactions (blue pathways, Scheme 1) to form other alkene products $(C_{n\neq 6})$. Higher-rank reactions include the oligomerization of propene and C_6 to form trimers (C_9) , their subsequent oligomerization to heavier alkenes (i.e., $C_{n>9}$), and β -scission reactions of oligomers $(C_{n\geq 9})$ to form smaller fragments. Selectivities to the primary product (S_{C_6}) and to products formed in higher-rank reactions $(S_{C_{HR}})$, eq 5) were determined by

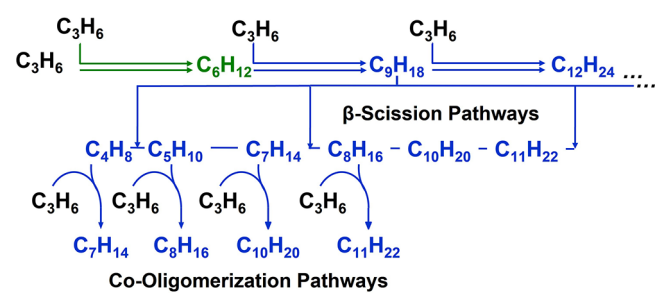
$$S_{C_{HR}} = \frac{r_n}{r_n + r_6} \tag{5}$$

In eq 5, r_n is the measured rate of formation of an alkene product of carbon number n ($n \neq 3$, 6) and r_6 is the measured rate of formation of C_6 alkenes.

Selectivities to the primary (S_{C_6}) and higher-rank $(S_{C_{HR}})$ products were measured for MFI samples of fixed crystallite size (\sim 0.3 μ m) but varied H⁺-site density, to determine the effect of H⁺-site density on the fraction of dimers undergoing

Scheme 1. Propene Oligomerization Reaction Network on H-Zeolites^a

Oligomerization Pathway



"Figure adapted from Bickel and Gounder. Oligomerization products defined as those whose carbon numbers are integer multiples of propene (i.e., $C_{3i}H_{2(3i)}$, i=2,3,4,...). Blue products and arrows indicate secondary and higher-rank reaction pathways, which are prevalent on MFI samples of low H⁺-site density relative to samples of higher H⁺-site densities. The green pathway denotes dimerization to form the primary reaction product (C_6).

higher-rank reactions. The selectivity to dimers and higher-rank products is shown as a function of propene conversion at two representative propene pressures of 16 and 315 kPa in Figure 5a,c, respectively. For all samples and reaction conditions, increasing conversions led to decreasing selectivity to the primary product and increasing selectivity to higher-rank reaction products (Figure 5a,c). This dependence is consistent with higher fluid-phase concentrations of the primary product at higher conversions, which in turn increase rates of higher-rank reactions. A Notably, decreasing conversion in Figure 5 also corresponds to increasing time-on-stream. Increasing selectivity to C_6 for MFI samples with increasing time-on-stream is consistent with our previously reported data on MFI samples of dilute H^+ -site density (\sim 0.3 H^+ /u.c.).

The ratio of higher-rank-to-primary product selectivity $(S_{C_{HR}}/S_{C_6})$ at fixed conversion is plotted against H⁺-site density at 16 and 315 kPa C_3H_6 in Figure 5b,d, respectively. Selectivity ratios of higher-rank to dimer products $(S_{C_{HR}}/S_{C_6})$ at low propene pressures (e.g., 16 kPa, Figure 5a,b) were similar (within ca. 1.15×) among MFI samples of varied H⁺-site

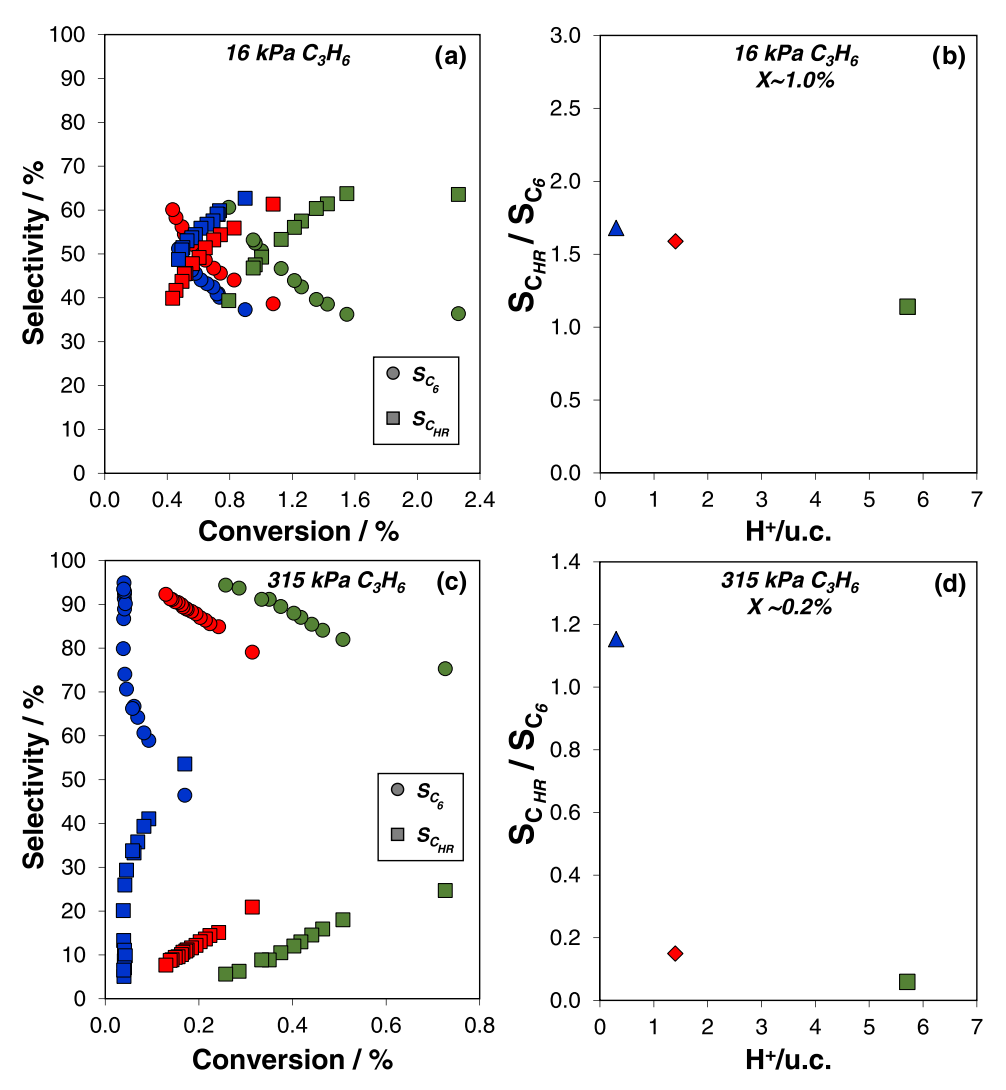


Figure 5. Product selectivity to C_6 (circles), and higher-rank reaction products ($S_{C_{HR}}$, eq 5) (squares) measured at 503 K and (a) 16 kPa and (c) 315 kPa C_3H_6 . The ratio of selectivity of higher-rank reaction products to dimers ($S_{C_{HR}}/S_{C_6}$) measured at 503 K and (b) 16 kPa and (d) 315 kPa C_3H_6 on MFI samples of varied Al content: MFI-0.3-0.31 (blue), MFI-1.3-0.33 (red), and MFI-5.7-0.30 (green). Uncertainty on selectivity is $\pm 2\%$. Decreasing conversion corresponds to increasing time-on-stream.

density when compared at fixed conversion. In contrast, significant differences in selectivity ratios were observed at higher propene pressures (e.g., 315 kPa, Figure 5c) among MFI samples of varied H⁺-site density. Lower-H⁺-site-density samples showed significantly higher selectivity to higher-rank reaction products than higher-H⁺-site-density samples, despite comparatively lower conversions (e.g., 50% at X=0.2% for MFI-0.3-0.31 vs 5% at X=0.3% for MFI-5.7-0.30, Figure 5c), and higher ratios of higher-rank-to-dimer products at isoconversion (Figure 5d). Similar trends in selectivity were observed over a wide range of propene pressures in the high-pressure limit (165–607 kPa C_3H_6 , further discussion in Section S10, SI).

The formation of larger fractions of higher-rank reaction products on MFI samples of more dilute H⁺-site density (Figure 5c) contrasts the expected correlation between selectivity and H⁺-site density when H⁺ sites among all MFI samples possess equal reactivity. In such a case, dimers formed in samples of higher H⁺-site density would have longer intracrystalline residence times (per H⁺); consequently, a greater quantity of dimers should undergo higher-rank

reactions (e.g., trimerization, β -scission) during their diffusion through a crystallite of higher H+-site density. Thus, the observed increases in selectivity to higher-rank reaction products with decreasing H+-site density indicate that rates of higher-rank reactions are faster on samples of lower H⁺-site density. Trimerization, the formation of C9 from the reaction of C₆ and propene, is the first higher-rank reaction in the propene oligomerization reaction network (Scheme 1) and precedes all other higher-rank reactions (e.g., tetramerization, β -scission, Scheme 1). Thus, greater selectivity to higher-rank reaction products, as observed on MFI samples of dilute H+site density, indicates that the rate of trimerization relative to dimerization is higher for these samples, resulting in larger fractions of dimers undergoing higher-rank reactions. The rate of formation of C9 depends on the concentrations of propene and C_6 , and the effective rate constant for trimerization (eq S8, SI). Since selectivities are measured at fixed fluid-phase propene concentrations, higher rates of trimerization on MFI samples of lower H+-site density suggest that the effective kinetic trimerization rate constant is higher for these samples. Notably, this conclusion is consistent with the proposal of Mlinar et al., who reported higher DFT-estimated activation enthalpies for trimerization relative to dimer desorption in MFI (by ca. 80 kJ mol^{-1} , T_{12}) in the presence of a proximal C_6 adsorbate, and hypothesized that rates of trimerization steps will be lower for MFI samples of higher Al content, which possess on average higher H⁺-site proximity. Thus, we conclude that rates of trimerization relative to dimerization are higher on MFI samples of lower H⁺-site density, resulting in greater fractions of dimer products undergoing trimerization and other higher-rank reactions.

Differences in reaction pathways and product composition on MFI samples of varied H+-site density are illustrated in Scheme 1. Blue arrows indicate higher-rank reaction pathways, which prevail on MFI samples of lower H+-site density compared to samples of higher H+-site density at higher propene pressures (≥165 kPa C₃H₆). Differences in gas-phase product distributions and prevalent reaction pathways among MFI samples of varied H+-site density indicate that the composition of the occluded organic phase also differs among these samples. The presence of intrazeolite mass transfer limitations precludes equating gas-phase product distributions with the composition of the occluded organic phase; however, changes in product selectivity can indirectly evidence changes in the composition of occluded products. Higher rates of trimerization and higher selectivity to higher-rank reaction products on MFI samples of dilute H+-site density indicate faster formation of heavier oligomer products $(C_{n>9})$, and consequently larger quantities of higher-molecular-weight products occluded within these samples. Thus, the differences in selectivity among MFI samples of varied H+-site density suggest that the composition of the occluded organic phase will become increasingly heavy in composition with decreasing H⁺site density at higher propene pressures.

Differences in the composition of the occluded organic phase among MFI samples of varied H⁺-site density rationalize the dependence of ξ (eq 4) on H⁺-site density (Figure 4a). The effective diffusivity of propene and product alkenes is influenced by the composition of the intrazeolite organic phase formed during propene oligomerization. The large fractions of heavier products formed in MFI samples of dilute H+-site density restrict intrazeolite diffusion, resulting in lower effective diffusivities of propene and product alkenes in these samples. Consequently, the value of ξ decreases with increasing H⁺/u.c. at higher propene pressures. At lower propene pressures, product compositions are similar among MFI samples of all H⁺-site densities, suggesting the effective diffusivities of propene and product alkenes will also be similar among these MFI samples under these reaction conditions. Thus, differences in ξ at low propene pressures likely reflect differences in the effective dimerization rate constant among MFI samples of varied H⁺-site density. Values of ξ are higher for MFI samples of more dilute H⁺-site density at low propene pressures (Figure 4b), suggesting these samples have higher effective dimerization rate constants. We conclude that MFI samples of lower H+-site contents possess higher effective dimerization rate constants, but also higher rate constants for other oligomerization reactions (e.g., trimerization), leading to the formation higher-molecular-weight products within their micropores and consequently lower effective diffusivities of propene and product alkenes.

3.4. Influence of H⁺-Site Density on Apparent Propene Dimerization Reaction Orders. Steady-state propene dimerization rates were measured at varied propene

pressure for MFI samples of different H⁺-site densities (Figure 6). Apparent dimerization reaction orders differed among MFI

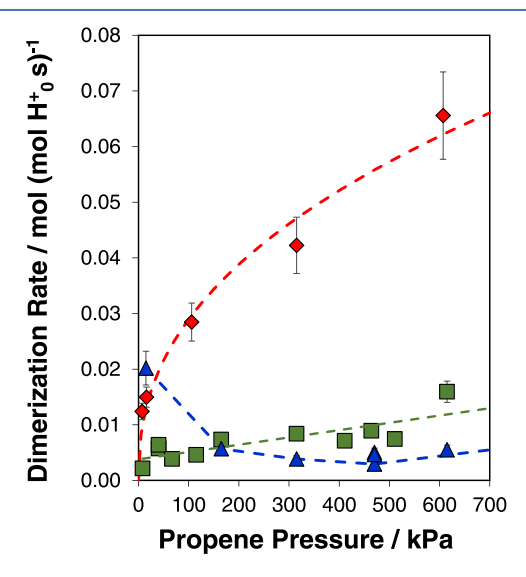


Figure 6. Steady-state propene dimerization rates (503 K) measured on MFI-0.3-0.31 (triangles), MFI-1.3-0.06 (diamonds), and MFI-5.7-0.30 (squares) at varied propene pressure. Dashed lines are a guide to the eye.

samples of different H⁺-site densities (MFI-0.3-0.31, MFI-1.3-0.06, MFI-5.7-0.30). Dimerization rates measured on the lowest-H⁺-site-density sample (MFI-0.3-0.31, Figure 6, triangles) were initially negative order in propene pressure and became slightly more positive order at higher propene pressures, consistent with our previous findings for an MFI sample of dilute H+-site density but smaller crystallite size.8 In contrast, dimerization rates measured on an MFI sample of higher H⁺-site density (MFI-1.3-0.06, Figure 6, diamonds) increased systematically with propene pressure, although this increase was attenuated at higher propene pressures. Dimerization rates measured on the highest-H+-site-density sample (MFI-5.7-0.30, Figure 6, squares) increased linearly with propene pressure, although a linear regression to these data extrapolated to a finite dimerization rate at zero propene pressure. Apparent dimerization reaction orders were similar among MFI samples of fixed H+-site density and varied crystallite size (Figure S16, SI), indicating that differences in reaction orders are a consequence of changes to the H+-site density.

Different apparent reaction orders among MFI samples of varied H⁺-site density can be rationalized by considering the convoluted influences of kinetics and intrazeolite diffusional constraints imposed by occluded hydrocarbon products on measured dimerization rates. A first-order dependence of dimerization rate on propene pressure is expected regardless of the identity of the species assumed to be the most-abundant surface intermediate (MASI) over a given range of propene pressures in the limit of kinetic control (further discussion in Section S12, SI).⁸ Thus, changes in the kinetic regime cannot rationalize the reaction orders observed in Figure 6 or the changes in reaction order among MFI samples of different H⁺-site densities. Consequently, changes in reaction order with H⁺-site density must reflect differences in intrazeolite diffusional constraints on dimerization rates, which can arise from

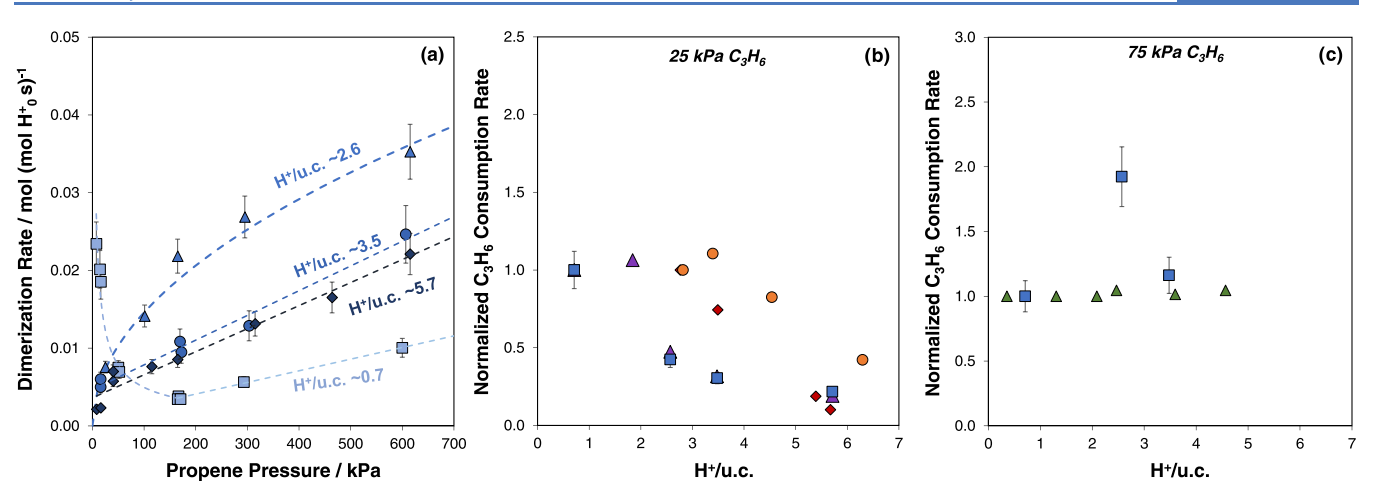


Figure 7. (a) Dimerization rates (503 K) measured after 12 ks time-on-stream on commercial H-MFI samples of varied $H^+/u.c.$ also studied in previous reports^{2,3,7} plotted against propene pressure. Dashed lines indicate interpolations of measured rate data and are extrapolated to a higher pressure to guide the eye. (b) Normalized propene consumption rates measured on commercial MFI samples by Mlinar et al.² (513 K, 25 kPa C_3H_6 , triangles), on MFI samples crystallized with <22% proximal Al by Bernauer et al.³ (533 K, 22 kPa C_3H_6 , circles), on MFI samples crystallized with >72% proximal Al by Bernauer et al.³ (533 K, 22 kPa C_3H_6 , diamonds), and determined by interpolation in this work (503 K, 25 kPa C_3H_6 , squares). (c) Normalized propene consumption rates measured on commercial MFI samples by Sarazen et al.⁷ (503 K, 75 kPa C_3H_6 , triangles) and determined by interpolation in this work (503 K, 25 kPa C_3H_6 , squares). Notably, the commercial MFI sample with the lowest Al content is also the same commercial sample with the lowest $H^+/u.c.$ tested by Sarazen et al.⁷ but the value of $H^+/u.c.$ measured in that study differed from that measured herein. Normalized rates were acquired by normalizing the propene consumption rates in each study by the rate measured on the MFI sample of the lowest H^+ -site density in each study.

changes in the composition of the occluded organic phase with propene pressure and H⁺-site density.

Differences in intrazeolite diffusional constraints among MFI samples of varied H⁺-site density reflect the different influences of propene pressure on the composition of the occluded organic phase, and consequently on the effective diffusivities of propene and product alkenes among these samples. Concentrations of higher-molecular-weight products increase within the occluded organic phase with increasing propene pressure⁸ for MFI samples of all H+-site densities (Sections 3.1 and S11, SI) and thereby lower the effective diffusivity of propene and product alkenes (Figure 4a). Higher propene pressures increase the kinetic rate of dimerization (eq S5, SI); however, the concomitant decrease in effective diffusivity with propene pressure results in greater intrazeolite diffusional constraints. Thus, measured dimerization rates will decrease with increasing propene pressure when the decrease in the rate of intrazeolite diffusion is more significant than the increase in the kinetic rate, and increase with increasing propene pressure when the increase in the kinetic rate is more significant than the decrease in the rate of intrazeolite diffusion.

The different reaction orders observed among MFI samples of varied H⁺-site density reflect the different extents to which the effective diffusivity decreases with increasing propene pressure among these samples. Larger fractions of the occluded organic phase are composed of heavier oligomers with increasing propene pressure on MFI samples of lower H⁺-site density, as evidenced by higher selectivities to higher-rank products (Figure 5 and Section S11, SI) and the comparatively large decrease in the effective diffusivity with increasing propene pressure (ξ decreases by >10²×, Figure 4a) for these samples. In contrast, the growth of higher-molecular-weight oligomers with increasing propene pressure is restricted in MFI samples of higher H⁺-site density (Figure 5 and Section S11, SI), resulting in an attenuated decrease in effective diffusivity with increasing propene pressure (by < 10× for

MFI-5.7-0.30, Figure 4a). The large decrease in effective diffusivity with increasing propene pressure on MFI samples of low H+-site density (Figure 4a, triangles) results in a disproportionately large increase in diffusional constraints with increasing propene pressure, and consequently, the negative apparent reaction order observed for MFI-0.3-0.31 in Figure 6. In contrast, the attenuated decrease in effective diffusivity with increasing propene pressure for MFI samples of the highest H+-site density studied (MFI-5.7-0.30) leads to apparent reaction orders that more closely resemble the firstorder dependence of dimerization rate on propene pressure that is expected in the limiting case wherein effective diffusivities remain constant with changing propene pressure. Notably, even a continuous first-order dependence of dimerization rates on propene pressure would not indicate that rates are kinetically limited, but only that the effective diffusivities of propene and product alkenes do not vary significantly with propene pressure. Dimerization rates (per H⁺) that are independent of crystallite size for samples of fixed H⁺-site density, when compared in the same kinetic regime, are necessary to evidence the absence of diffusional constraints, as established in the conceptual frameworks of the Koros-Nowak and Madon-Boudart criteria. 25,26 Overall, we conclude that H+-site density and propene pressure distinctly influence the composition of the occluded organic phase, and in turn the effective diffusivities of propene and product alkenes, resulting in apparent reaction orders that deviate from the first-order dependence expected in the limit of kinetic control and that vary among MFI samples of varied H⁺-site density.

Accounting for the influence of H⁺-site density on the effective diffusivity of propene and product alkenes and the coupled influences of kinetics and transport on measured propene oligomerization rates also allows rationalizing the contrasting dependences of propene oligomerization rate on H⁺-site density reported in previous studies.^{2,3,7} Four MFI samples were obtained from commercial sources (Table S4,

SI), which were nominally the same materials studied in previous reports (further discussion in Section S13, SI). 2,7 Commercial MFI samples of different H⁺-site densities exhibited different apparent dependences of dimerization rate on propene pressure, as shown in Figure 7a. Dimerization rates measured on MFI samples of higher H⁺-site density exhibited a positive-order dependence on propene pressure, while rates measured on the MFI sample of most dilute Al (Si/Al ~140, H⁺/u.c. ~0.6) exhibited a negative-order dependence. The differences in apparent reaction orders among commercial MFI samples of H⁺-site density are consistent with the changes in reaction order with H⁺-site density observed for MFI-X-Y samples herein (Figure 5).

Rates of propene consumption for these samples were also estimated (further discussion in Section S13, SI) at the two different propene pressures examined in prior studies (~25 and 75 kPa) to compare the dependence of rates on H⁺-site density measured for commercial MFI samples herein against that measured in previous reports.^{2,7} To enable comparison despite the small differences in reaction temperature among these studies $(\sim 20 \text{ K})$, $^{2-4}$ rates from each study were normalized by the rate measured at the lowest H+-site density in that study. At low propene pressures (25 kPa), rates decreased systematically with increasing H+/u.c. (Figure 7b), in agreement with the findings of Mlinar et al.2 for nominally the same commercial MFI samples (Figure 7b, triangles) and with the findings of Bernauer et al.³ (Figure 7b, circles and diamonds). Notably, rate differences among these samples cannot be directly attributed to differences in H+-site density because crystallite sizes vary among these samples (Figure S18, SI); however, higher rates on samples of low H⁺/u.c. primarily reflect the comparatively higher rates measured for MFI samples of dilute H+-site density at low propene pressures in the negative-order regime (Figures 7a and S17, SI). In contrast, dimerization rates measured at a higher propene pressure (75 kPa) do not correlate with H+-site density, and appear independent of H+/u.c., in agreement with the findings of Sarazen et al. (Figure 7c). At this pressure, dimerization rates coincide between two MFI samples of high and low H+-site density (H+/u.c. 0.7 and 3.5), despite the different reaction orders among these samples observed over a much wider range of propene pressures (Figure 7a).

We conclude that the different dependences of propene oligomerization rates on H⁺-site density reported previously for rates measured at fixed, but different, values of propene pressure are irreconcilable if propene consumption rates are assumed to be kinetically controlled and measured in the same kinetic regime. However, accounting for the influence of intrazeolite diffusional constraints and their dependence on propene pressure and H+-site density can satisfactorily rationalize these differences. The influence of intrazeolite diffusion limitations imposed by the occluded organic phase and the dependence of the composition of this phase on propene pressure and H+-site density results in different reaction orders among samples of different H+-site density (Figure 7a). These reaction orders cannot be rationalized or predicted by kinetic rate laws alone,8 but can be explained when considering the coupled influences of kinetics and transport barriers imposed by occluded oligomerization products on measured rates, and their dependence on H+site density.

4. CONCLUSIONS

Both kinetic factors and intrazeolite diffusional constraints influence measured rates and selectivities of propene oligomerization on MFI zeolites of widely varying composition $(H^+/u.c.~0.3-5.7)$ and crystallite size $(0.03-2.69~\mu m)$. The ubiquitous influence of intrazeolite diffusional constraints among these materials is evidenced by dimerization rates (per H⁺) that decrease systematically with increasing crystallite size for samples of fixed H+-site density and with a functional dependence consistent with the prediction of the effectiveness factor formalism in the limit of strong intrazeolite mass transfer limitations. Regeneration experiments with inert gas, in conjunction with transient changes in dimerization rate upon step-changes in propene pressure and reaction temperature, indicate that these intrazeolite diffusional constraints arise because heavier alkene products become occluded within the zeolitic micropores during reaction and lower the effective diffusivities of propene and product alkenes within MFI

Propene oligomerization reactions performed on suites of MFI samples synthesized with fixed H⁺-site density (0.3, 1.3, 5.7 H⁺/u.c.) and varied crystallite size (0.03–2.65 μ m) revealed the strong influence of H+-site density on the composition of occluded products, and thereby propene oligomerization rates and selectivity. For MFI samples of all compositions, the effective diffusivity of propene and product alkenes systematically decreased with increasing propene pressure because higher propene pressures result in higher concentrations of heavier products within the occluded organic phase; however, the decrease in effective diffusivity with increasing propene pressure was attenuated for MFI samples of higher H⁺-site density. Lower selectivities to higher-rank products on MFI samples of higher H+-site density indicate that this attenuated decrease reflects their lower reactivities for the growth of higher-molecular-weight oligomers (e.g., C9, C₁₂) compared to samples of more dilute H⁺-site density. Effective dimerization rate constants are higher for MFI samples of lower H+-site density; however, the greater concentrations of higher-molecular-weight oligomer products formed in MFI samples of low H+-site density at higher pressures impose disproportionately severe diffusional restrictions on propene and product alkenes.

The influence of H⁺-site density on the composition of the occluded organic phase results in different apparent reaction orders among MFI samples of varied H+-site density. The more facile growth of higher-molecular-weight alkenes with increasing propene pressure on MFI samples of dilute H+-site density results in a disproportionately large decrease in effective diffusivity compared to the increase in kinetic rate with increasing propene pressure for these samples. Consequently, dimerization rates measured on MFI samples of dilute H⁺-site density exhibit negative apparent reaction orders in propene pressure. The more restricted growth of heavier products on MFI samples of higher H+-site density results in an attenuated decrease in effective diffusivity with increasing propene pressure, and consequently, reaction orders that are more positive-order in propene pressure and approach the first-order dependence expected from kinetic rate laws when effective diffusivity does not change considerably with propene pressure.

Importantly, the influence of H⁺-site density on the composition of the occluded organic phase results in different

dependences of propene dimerization rate on H⁺-site density at low and high propene pressures, rationalizing the different dependences of propene consumption rates on H+-site density reported in previous studies of propene oligomerization at fixed but different pressures, 2,3,7 which are contradictory if dimerization rates are governed only by kinetic factors. The critical influence of intrazeolite diffusional constraints on measured rates during light alkene oligomerization and the influence of H+-site density on these constraints has gone unidentified in these studies, in large part because of concomitant changes in crystallite size and H+-site density among commercially sourced MFI samples, and because values of the Weisz-Prater criterion estimated with the singlecomponent effective diffusivity of the reactant alkene 2,7,9 indicate intrazeolite diffusional constraints should not be present. Our findings indicate that when the presence of products within zeolitic micropores influences effective diffusivity, the presence of intrazeolite diffusion limitations can only be revealed by examining the dependence of rate on crystallite size in materials where other catalyst properties (e.g., H+-site density) are fixed.

This study, together with our previous work,8 demonstrates the critical role of intrazeolite diffusional constraints resulting from occluded alkene products in governing the measured rates and selectivities of propene oligomerization. The composition of this occluded organic phase is sensitive to H⁺-site density, providing additional opportunities to tailor the rate and selectivity of propene oligomerization on H-MFI zeolites. More broadly, these findings demonstrate the imposition of intrazeolite diffusion limitations by slowly diffusing products and the influence of H+-site density in MFI on both the formation and composition of such products, providing a framework to diagnose and quantify the possible presence of such influences in other zeolite-catalyzed chaingrowth reactions (e.g., methanol-to-hydrocarbons)^{27,28} that form heavier and slowly diffusing intermediate and product molecules.

ASSOCIATED CONTENT

Supporting Information

The Supporting Information is available free of charge at https://pubs.acs.org/doi/10.1021/acscatal.2c05184.

Characterization data for zeolite samples (XRD, N_2 adsorption NH_3 temperature-programmed desorption, elemental analysis) as well as supplemental propene oligomerization reaction data and discussion (PDF)

AUTHOR INFORMATION

Corresponding Author

Rajamani Gounder — Charles D. Davidson School of Chemical Engineering, Purdue University, West Lafayette, Indiana 47907, United States; orcid.org/0000-0003-1347-534X; Email: rgounder@purdue.edu

Authors

Elizabeth E. Bickel – Charles D. Davidson School of Chemical Engineering, Purdue University, West Lafayette, Indiana 47907, United States

Songhyun Lee – Charles D. Davidson School of Chemical Engineering, Purdue University, West Lafayette, Indiana 47907, United States

Complete contact information is available at:

https://pubs.acs.org/10.1021/acscatal.2c05184

Author Contributions

The manuscript was written through contributions of all authors, and all authors have given approval to the final version of the manuscript.

Notes

The authors declare no competing financial interest.

ACKNOWLEDGMENTS

The authors acknowledge financial support provided by the National Science Foundation under Cooperative Agreement No. EEC-1647722, which is an Engineering Research Center for the Innovative and Strategic Transformation of Alkane Resources. They also acknowledge helpful technical discussions with Professor David Hibbitts (University of Florida). They thank Lauren Kilburn and Dr. Mykela DeLuca (Purdue) for helpful technical discussions and for providing a critical review of this manuscript.

REFERENCES

- (1) Degnan, T. F., Jr. Applications of Zeolites in Petroleum Refining. *Top. Catal.* **2000**, *13*, 349–356.
- (2) Mlinar, A. N.; Zimmerman, P. M.; Celik, F. E.; Head-Gordon, M.; Bell, A. T. Effects of Brønsted-Acid Site Proximity on the Oligomerization of Propene in H-MFI. *J. Catal.* **2012**, 288, 65–73.
- (3) Bernauer, M.; Tabor, E.; Pashkova, V.; Kaucký, D.; Sobalík, Z.; Wichterlová, B.; Dedecek, J. Proton Proximity New Key Parameter Controlling Adsorption, Desorption and Activity in Propene Oligomerization over H-ZSM-5 Zeolites. *J. Catal.* **2016**, 344, 157–172.
- (4) Sarazen, M. L.; Doskocil, E.; Iglesia, E. Effects of Void Environment and Acid Strength on Alkene Oligomerization Selectivity. *ACS Catal.* **2016**, *6*, 7059–7070.
- (5) Corma, A.; Martínez, C.; Doskocil, E. Designing MFI-Based Catalysts with Improved Catalyst Life for C3 = andC5 = Oligomerization to High-Quality Liquid Fuels. *J. Catal.* **2013**, *300*, 183–196.
- (6) Tabor, E.; Bernauer, M.; Wichterlová, B.; Dedecek, J. Enhancement of Propene Oligomerization and Aromatization by Proximate Protons in Zeolites; FTIR Study of the Reaction Pathway in ZSM-5. *Catal. Sci. Technol.* **2019**, *9*, 4262–4275.
- (7) Sarazen, M. L.; Doskocil, E.; Iglesia, E. Catalysis on Solid Acids: Mechanism and Catalyst Descriptors in Oligomerization Reactions of Light Alkenes. *J. Catal.* **2016**, *344*, 553–569.
- (8) Bickel, E. E.; Gounder, R. Hydrocarbon Products Occluded within Zeolite Micropores Impose Transport Barriers That Regulate Brønsted Acid-Catalyzed Propene Oligomerization. *JACS Au* **2022**, *2*, 2585–2595.
- (9) Wulfers, M. J.; Lobo, R. F. Assessment of Mass Transfer Limitations in Oligomerization of Butene at High Pressure on H-Beta. *Appl. Catal., A* **2015**, *505*, 394–401.
- (10) de Klerk, A. Oligomerization of 1-Hexene and 1-Octene over Solid Acid Catalysts. *Ind. Eng. Chem. Res.* **2005**, *44*, 3887–3893.
- (11) Lee, S.; Choi, M. Unveiling Coke Formation Mechanism in MFI Zeolites during Methanol-to-Hydrocarbons Conversion. *J. Catal.* **2019**, *375*, 183–192.
- (12) Kim, K.; Ryoo, R.; Jang, H.-D.; Choi, M. Spatial Distribution, Strength, and Dealumination Behavior of Acid Sites in Nanocrystalline MFI Zeolites and Their Catalytic Consequences. *J. Catal.* **2012**, 288, 115–123.
- (13) Nimlos, C. T.; Hoffman, A. J.; Hur, Y. G.; Lee, B. J.; Di Iorio, J. R.; Hibbitts, D. D.; Gounder, R. Experimental and Theoretical Assessments of Aluminum Proximity in MFI Zeolites and Its Alteration by Organic and Inorganic Structure-Directing Agents. *Chem. Mater.* **2020**, 32, 9277–9298.

- (14) Costa, C.; Lopes, J. M.; Lemos, F.; Ramôa Ribeiro, F. Activity-Acidity Relationship in Zeolite Y: Part 1. Transformation of Light Olefins. J. Mol. Catal. A: Chem. 1999, 144, 207-220.
- (15) Vernuccio, S.; Bickel, E. E.; Gounder, R.; Broadbelt, L. J. Microkinetic Model of Propylene Oligomerization on Brønsted Acidic Zeolites at Low Conversion. ACS Catal. 2019, 9, 8996-9008.
- (16) Weisz, P. B.; Prater, C. D.Interpretation of Measurements in Experimental Catalysis. In Advances in Catalysis; Frankenburg, W. G.; Komarewsky, V. I.; Rideal, E. K., Eds.; Academic Press, 1954; Vol. 6, pp 143-196. DOI: 10.1016/S0360-0564(08)60390-9.
- (17) Masuda, T.; Okubo, Y.; Mukai, S. R.; Kawase, M.; Hashimoto, K.; Shichi, A.; Satsuma, A.; Hattori, T.; Kiyozumi, Y. Effective Difusivities of Lighter Hydrocarbons in Cu- and Co-MFI-Type Zeolite Catalysts. Chem. Eng. Sci. 2001, 56, 889-896.
- (18) Díaz, M.; Epelde, E.; Valecillos, J.; Izaddoust, S.; Aguayo, A. T.; Bilbao, J. Coke Deactivation and Regeneration of HZSM-5 Zeolite Catalysts in the Oligomerization of 1-Butene. Appl. Catal., B 2021, 291. No. 120076.
- (19) Dimon, B.; Cartraud, P.; Magnoux, P.; Guisnet, M. Coking, Aging and Regeneration of Zeolites: XIV. Kinetic Study of the Formation of Coke from Propene over USHY and H-ZSM-5. Appl. Catal., A 1993, 101, 351-369.
- (20) Quann, R. J.; Green, L. A.; Tabak, S. A.; Krambeck, F. J. Chemistry of Olefin Oligomerization over ZSM-5 Catalyst. Ind. Eng. Chem. Res. 1988, 27, 565-570.
- (21) Martínez, C.; Corma, A. Inorganic Molecular Sieves: Preparation, Modification and Industrial Application in Catalytic Processes. Coord. Chem. Rev. 2011, 255, 1558-1580.
- (22) Garwood, W. E.Conversion of C2 -C10 to Higher Olefins over Synthetic Zeolite ZSM-5. In Intrazeolite Chemistry; Stucky, G. D.; Dwyer, F. G., Eds.; American Chemical Society: Washington, D.C, 1983; Vol. 218, pp 383-396. DOI: 10.1021/bk-1983-0218.ch023.
- (23) Cnudde, P.; Redekop, E. A.; Dai, W.; Porcaro, N. G.; Waroquier, M.; Bordiga, S.; Hunger, M.; Li, L.; Olsbye, U.; Van Speybroeck, V. Experimental and Theoretical Evidence for the Promotional Effect of Acid Sites on the Diffusion of Alkenes through Small-Pore Zeolites. Angew. Chem., Int. Ed. 2021, 60, 10016-10022.
- (24) Bhore, N. A.; Klein, M. T.; Bischoff, K. B. The Delplot Technique: A New Method for Reaction Pathway Analysis. Ind. Eng. Chem. Res. 1990, 29, 313-316.
- (25) Koros, R. M.; Nowak, E. J. A Diagnostic Test of the Kinetic Regime in a Packed Bed Reactor. Chem. Eng. Sci. 1967, 22, 470.
- (26) Madon, R. J.; Boudart, M. Experimental Criterion for the Absence of Artifacts in the Measurement of Rates of Heterogeneous Catalytic Reactions. Ind. Eng. Chem. Fund. 1982, 21, 438-447.
- (27) Hwang, A.; Le, T. T.; Shi, Z.; Dai, H.; Rimer, J. D.; Bhan, A. Effects of Diffusional Constraints on Lifetime and Selectivity in Methanol-to-Olefins Catalysis on HSAPO-34. J. Catal. 2019, 369, 122 - 132.
- (28) Shen, Y.; Le, T. T.; Fu, D.; Schmidt, J. E.; Filez, M.; Weckhuysen, B. M.; Rimer, J. D. Deconvoluting the Competing Effects of Zeolite Framework Topology and Diffusion Path Length on Methanol to Hydrocarbons Reaction. ACS Catal. 2018, 8, 11042-11053.

□ Recommended by ACS

Solvent Mediated Interactions on Alkene Epoxidations in Ti-MFI: Effects of Solvent Identity and Silanol Density

Chris Torres, David W. Flaherty, et al.

ILINE 21 2023 ACS CATALYSIS

READ 2

Combining Theoretical and Experimental Methods to Probe Confinement within Microporous Solid Acid Catalysts for **Alcohol Dehydration**

Matthew E. Potter, Lindsay-Marie Armstrong, et al.

APRIL 17, 2023 ACS CATALYSIS

READ **C**

Untangling Framework Confinements: A Dynamical Study on Bulky Aromatic Molecules in MFI Zeolites

Yi Ji, Guangjin Hou, et al.

NOVEMBER 29, 2022

ACS CATALYSIS

RFAD 17

Effect of Diffusion Constraints and ZnO_x Speciation on Nonoxidative Dehydrogenation of Propane and Isobutane over ZnO-Containing Catalysts

Dan Zhao, Evgenii V. Kondratenko, et al.

FEBRUARY 22, 2023

ACS CATALYSIS

RFAD 🗹

Get More Suggestions >